Shearlet-TGV Based Fluorescence Microscopy Image Deconvolution

Jing Qin[1], Xiyu Yi[2], Shimon Weiss[2], and Stanley Osher[1]

[1] Department of Mathematics, University of California, Los Angeles, CA 90095
[2] Department of Chemistry, University of California, Los Angeles, CA 90024

Abstract. With the recent advent of superresolution imaging methodologies, various deconvolution algorithms have been applied to fluorescence microscopy images to enhance the image resolution, including non-blind approaches requiring elaborate experiments to precisely measure the optical point spread function (PSF), and blind approaches which estimate PSF from the image itself. Recently, the superresolution optical fluctuation imaging (SOFI) has been developed and provided a fast estimation of PSF which can be directly used in some post-processing non-blind or prior-guided blind deconvolution algorithms. In this paper, we propose a novel regularization based image deconvolution approach, which combines the shearlet transform and total generalized variation (TGV) to further enhance the SOFI results. This method could presumably be useful for other diffraction-limited and superresolution imaging modalities. Since the quality of the estimated PSF by SOFI may vary, we propose both a non-blind deconvolution version and a prior-guided blind deconvolution version. We tested the performance of our deconvolution algorithms on simulated images with microtubule-like structures. Our approach is efficient in representing directional thin structures, e.g., the microtubules, and it preserves high order image smoothness. Due to these attributes it outperforms other state-of-the-art deconvolution methods for this class of morphologies.

Keywords: image deconvolution, SOFI, point spread function, shearlet transform, total generalized variation

1 Introduction

Deconvolution of fluorescence microscopy images, as a major post-processing step for visualizing sub-cellular structures at higher resolution has attracted attention in the image processing community. The fluorescence microscope produces blurred images due to the diffraction of light, imperfections in the optical system (including non-ideal PSF), dim signals, photobleaching, and large autofluoresence background. To address some of these issues, two categories of image deconvolution techniques have been developed: physical (optical) techniques that reduce the out-of-focus light, e.g., the confocal microscope, and computational techniques that utilize mathematical algorithms to improve image quality. The deconvolution performance can be improved by accounting for the measured,

non-ideal PSF. Although the PSF can in principle be accurately measured, it requires specialized equipment which slows down the work-flow and throughput.

Recently, the SOFI methodology [1] has been developed to enhance image resolution and contrast. As a by-product, it yields a fast and convenient estimation of PSF. The estimated PSF could be used for further image enhancement by non-blind or semiblind deconvolution. As a challenging ill-posed inverse problem, various methods have been proposed for image deconvolution, including Wiener filter [2], Richardson-Lucy algorithm [3, 4] based on the assumption that pixel intensity obeys the Poisson distribution, TV and nonlocal TV based approaches [5, 6], and multiscale transform based algorithms [7–10]. However, most of these algorithms suffer from losing distinctive directional features and/or creating artifacts in dealing with complicated microbiological images. Inspired by the capability of the shearlet transform in differentiating orientational features and TGV in preserving high order smoothness [11, 12], we propose a shearlet-TGV image deconvolution method in two versions: non-blind and PSF prior-guided. In contrast to building Wiener-type filters based on the shearlet transform in [9], the proposed method uses fixed parameters for all iterations and achieves fast convergence. To reduce the artifacts along fine features while preserving the layout of different line-shape fibers in the microscopy images of cells, the shearlet based regularization is imposed on the underlying image. By virtue of the PSF estimation in the SOFI methodology, a quadratic penalty involving an estimated PSF by SOFI and a regularization of PSF can be added to the non-blind deconvolution model to further assist image restoration. In addition, the proposed model is solved by an algorithm based on the alternating direction method of multipliers (ADMM, also known as split Bregman [13]), which guarantees the implementation efficiency with respect to the resultant image quality. A variety of numerical experiments show that our proposed algorithm has outstanding performance over some state-of-the-art methods in preserving the fine structures, especially the junctions of two curved lines.

The rest of the paper is organized as follows. In Section 2, we describe in detail the proposed shearlet-TGV based image deconvolution method in a non-blind version and one with PSF prior guidance. Performance comparisons with other popular deconvolution methods on synthetic data are presented in Section 3. In the end, we summarize the paper in Section 4.

2 Proposed Algorithm

Let $u : \Omega \to \mathbb{R}$ be the image of interest, where Ω is an open and bounded Lipschitz set in $\mathbb{R}^2$. The observed image $v : \Omega \to \mathbb{R}$ satisfies $v = h * u + n$, where h is a PSF and n is a Gaussian noise. In practice, the noise n may be either spatially variant or of unknown type. For simplicity, we assume that the noise n is homogeneous with variance σ^2. Given a known PSF h and the observed blurry image v, we consider the following minimization problem to restore the underlying image u

$$\min_u \frac{\mu}{2} \|h * u - v\|_2^2 + \Phi(u), \tag{1}$$

where $\Phi(u)$ is a regularization term, e.g., a TV seminorm $\int_\Omega |\nabla u|$ and a Besov norm involving certain multiscale transformation. We call (1) non-blind image deconvolution model. If the PSF is unknown, then the regularization with respect to the PSF h has to be taken into consideration and (3) turns into a blind image deconvolution model:

$$\min_{u,h} \frac{\mu}{2} \|h * u - v\|_2^2 + \Phi(u) + \Psi(h) \tag{2}$$

where $\Psi(h)$ is a regularization term to preserve some geometric properties of h. Since the PSF h corresponds to a point source in the fluorescence imaging system, we set $\Psi(h) = \|\nabla h\|_2^2$ to ensure the smoothness of h. In case of non-Gaussian noise as n, the L_2-norm in the data fidelity term can be replaced by a more robust L_1-norm.

2.1 Shearlet-TGV non-blind image deconvolution

Considering the sensitive orientation detection of shearlets [14] and preservation of high order image smoothness by TGV [15], we propose the shearlet-TGV nonblind image deconvolution model

$$\min_u \frac{\mu}{2} \|h * u - v\|_2^2 + \lambda \|\mathcal{SH}(u)\|_1 + \mathrm{TGV}_\alpha^2(u), \tag{3}$$

where $\mathcal{SH}(u)$ represents the shearlet transform of u. The second order TGV with weight $\alpha = (\alpha_0, \alpha_1)$ of u is defined as

$$\mathrm{TGV}_\alpha^2(u) = \sup \Big\{ \int_\Omega u \,\mathrm{div}^2 w \, dx \,\Big|\, w \in C_c^2(\Omega, S^{2\times 2}), \|w\|_\infty \le \alpha_0, \|\mathrm{div} w\|_\infty \le \alpha_1 \Big\}$$

where $S^{2\times 2}$ is the space of second order 2×2 symmetric matrices. By reformulating TGV as a minimizer in the discrete setting , the above model becomes

$$\min_{u,p} \frac{\beta}{2} \|h * u - v\|_2^2 + \lambda \|\mathcal{SH}(u)\|_1 + \alpha_1 \|\nabla u - p\|_1 + \alpha_0 \|\mathcal{E}(p)\|_1 . \tag{4}$$

where $\mathcal{E}$ is an operator defined in [15]. After applying the ADMM method, we get Algorithm 1. Similar to the algorithm in [12], the x-, y- and z-subproblems have closed-form solutions by using the generalized shrinkage operator. Rather than representing the convolution operator as a Toeplitz matrix, we obtain a closed-form solution for the least-squares (u, p)-subproblem by efficiently applying the fast Fourier transform.

2.2 Prior-guided shearlet based blind image deconvolution

SOFI provides a preprocessed deconvolved image and an estimated PSF $h_0(x)$, which can be treated as an approximation with high-accuracy to the actual PSF but with imperfections, i.e., the radius of a point source is enlarged or reduced.

Algorithm 1 Shearlet-TGV non-blind image deconvolution algorithm

1. Choose parameters $\mu_1, \mu_2, \mu_3, \beta, \lambda, \gamma, \alpha_1, \alpha_2$, initialize $\tilde{x}^0, \tilde{y}^0, \tilde{z}^0, u, p$.
2. For $n = 0, 1, 2, \ldots$, run the following computations

$$
\begin{aligned}
x^{n+1} &= \underset{x}{\operatorname{argmin}} \|x\|_1 + \frac{\mu_1}{2} \|x - \mathcal{SH}(u^n) - \tilde{x}^n\|_2^2, \\
y^{n+1} &= \underset{y}{\operatorname{argmin}} \|y\|_1 + \frac{\mu_2}{2} \|y - (Du^n - p^n) - \tilde{y}^n\|_2^2, \\
z^{n+1} &= \underset{z}{\operatorname{argmin}} \|z\|_1 + \frac{\mu_3}{2} \|z - \mathcal{E}(p^n) - \tilde{z}^n\|_2^2, \\
(u^{n+1}, p^{n+1}) &= \underset{u,p}{\operatorname{argmin}} \frac{\beta}{2} \|h * u - v\|_2^2 + \frac{\lambda\mu_1}{2} \left\|x^{n+1} - \mathcal{SH}(u) - \tilde{x}^n\right\|_2^2 \\
&\qquad + \frac{\alpha_1\mu_2}{2} \left\|y^{n+1} - (Du - p) - \tilde{y}^n\right\|_2^2 + \frac{\alpha_0\mu_3}{2} \|z - \mathcal{E}(p^n) - \tilde{z}^n\|_2^2, \\
\tilde{x}^{n+1} &= \tilde{x}^n + \gamma(\mathcal{SH}(u^{n+1}) - x^{n+1}) \\
\tilde{y}^{n+1} &= \tilde{y}^n + \gamma(Du^{n+1} - p^{n+1} - y^{n+1}), \\
\tilde{z}^{n+1} &= \tilde{z}^n + \gamma(\mathcal{E}(p^{n+1}) - z^{n+1}).
\end{aligned}
$$

   If the stopping criterion is satisfied, it stops.

By taking into account of machine noise, we propose the shearlet based blind image deconvolution with the prior knowledge of PSF:

$$
\min_{u,h} \lambda \|\mathcal{SH}(u)\|_1 + \mathrm{TGV}_\alpha^2(u) + \frac{\nu}{2} \|h - h_0\|_2^2 + \frac{\eta}{2} \|\nabla h\|_2^2 \quad \text{s.t.} \quad \|h * u - v\|_2 \le \sigma. \tag{5}
$$

To solve the constrained minimization problem (5), we apply ADMM and get

$$
\begin{cases}
u^{n+1} = \underset{u}{\operatorname{argmin}} \dfrac{\beta}{2} \|h^n * u - v + t^n\|_2^2 + \lambda \|\mathcal{SH}(u)\|_1 + \mathrm{TGV}_\alpha^2(u) \\
h^{n+1} = \underset{h}{\operatorname{argmin}} \dfrac{\nu}{2} \|h - h_0\|_2^2 + \dfrac{\eta}{2} \|\nabla h\|_2^2 + \dfrac{\beta}{2} \left\|h * u^{n+1} - v + t^n\right\|_2^2 \\
t^{n+1} = t^n + \gamma(v - h^{n+1} * u^{n+1}).
\end{cases} \tag{6}
$$

Note that the u-subproblem can be solved by applying Algorithm 1. Moreover, to solve the h-subproblem, we first pad h with zeros such that h is of the same matrix size as u and then apply the fast Fourier transform and get a closed-form solution

$$
h = \mathcal{F}^{-1}\left(\frac{\nu\mathcal{F}(h_0) + \beta\mathcal{F}(u^{n+1})^* \otimes \mathcal{F}(v - t^n)}{\nu + \eta\sum_{i=1}^2 \mathcal{F}(D_i)^* \otimes \mathcal{F}(D_i) + \beta\mathcal{F}(u)^* \otimes \mathcal{F}(u)}\right),
$$

where D_i are difference operators along x-direction and y-direction, and $\otimes$ is entry-wise matrix multiplication. To make the parameter tuning easier, the parameter β in the h-subproblem can be different from that in the u-subproblem.

3 Numerical Experiments

In this section, we present experimental results to show the performance of our approach on two synthetic images of size 200×200 simulating the Tubulin structures within a biological cell, and a PSF of size 100×100. All results are compared in terms of the *increase in signal to noise ratio* (ISNR) [16], which is defined as

$$ISNR = 10 \log_{10} \frac{N(v)}{N(u)}, \quad N(u) = \min_{a,b,\delta_x,\delta_y} \|au(\cdot + \delta_x, \cdot + \delta_y) + b - u_0\|_2^2$$

where the restored image u is obtained from the degraded blurry image v, u_0 is the ground truth and $u(\cdot + \delta_x, \cdot + \delta_y)$ represents the image u shifted by δ_x and δ_y in the horizontal and vertical directions respectively. By taking the spatial alignment and intensity scaling, this measure is more useful for comparing different deconvolution algorithms. To make comparison fair, we choose the optimal result for each method after parameter tuning. We fix $\mu_1 = 100$, $\mu_2 = \mu_3 = 0.01$, $\alpha_1 = 10$, $\alpha_2 = 0.001$ for all experiments, set γ as 0.1 for the first set of experiments and 1 for the second set, and choose optimal ν, λ from the set $\{0.1, 1, 10, 100\}$ for different noise levels and imperfection types of PSF.

In the first experiment, we generated curved lines from a random walk model which simulates microtubules-like structures in a cell. The ground truth u consists of multiple overlapping curved lines with randomly distributed emitters of line density 1.05 emitters per nanometer, cross-section marking uncertainty is 20 nm; the pixel size is 160 nm; h is simulated as a Gaussian PSF with the diffraction limit of 625 nm red laser. We test the data under three scenarios: 1) Gaussian noise with $\sigma = 3$ and perfect PSF, i.e., $v = h * u_0 + n$ and $n \sim \mathcal{N}(0, 9)$; 2) no noise and imperfect PSF with wider spatial support, i.e., $v = h * u_0$ and input PSF $\tilde{h} = h^{0.6}$; 3) Gaussian noise with $\sigma = 3$ and imperfect PSF, i.e., $v = h * u_0 + n$ and input PSF $\tilde{h} = h^{0.6}$. The imperfection of PSF is to simulate the estimation error of PSF in the SOFI system. We compare the proposed method with other competitive methods: Richardson-Lucy's method, statistical blind deconvolution method [17], i.e., "deconvblind" function in MATLAB, nonlocal TV [6] and framelet based deconvolution [10]. In addition, we test the recent algorithm proposed in [18], which fails to return an enhanced image due to the challenging dynamic range of the testing image. From the plots of ISNR versus the iteration number in Fig. 1 for each scenario, one can see that Richardson-Lucy's method is unstable but obtains a fairly good result, and our method shows the stable outstanding performance.

For the purpose of illustration, we show the results obtained under the most challenging scenario 3) in Fig. 2. The thin structures and junction parts are preserved due to the directional sensitivity of shearlets. In the meanwhile, the ringing artifacts along the geometric features are suppressed in our result from the contribution of TGV. In fact, the framelet based method has intensive artifacts at the scenario 3) which is implied by the ISNR plot. In order to show the robustness of the proposed model, we tested various noise levels $\sigma = 4, 6$ and imperfect PSFs $\tilde{h} = h^k$ with $k = 0.6, 0.8, 1, 1.2, 1.4$ in Table 1. It shows that our method consistently performs better than all other methods in terms of ISNR.

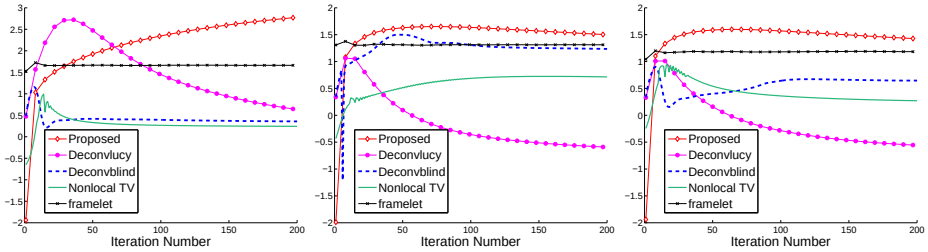

Fig. 1. From left to right: ISNR comparisons for blurry images with 1) Gaussian noise 2) imperfect PSF 3) Gaussian noise and imperfect PSF. The vertical axis represents ISNR.

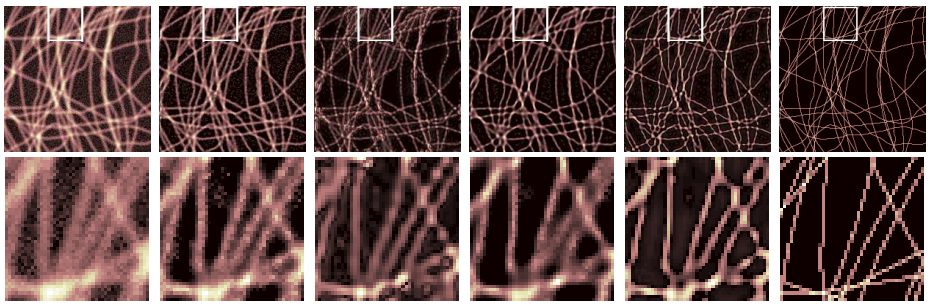

Fig. 2. Deconvolution of a blurry image with noise and imperfect PSF. From left to right: input blurry image, "deconvblind" (ISNR=0.90), nonlocal TV (ISNR=0.94), Richardson-Lucy (ISNR=1.06), proposed result (ISNR=1.60), and the ground truth.

	$\sigma = 4$					$\sigma = 6$				
k	0.6	0.8	1	1.2	1.4	0.6	0.8	1	1.2	1.4
Proposed	**1.48**	**2.76**	**2.88**	**2.23**	**1.96**	**1.48**	**2.13**	**2.03**	**1.67**	**1.46**
Richardson-Lucy	1.08	1.69	2.15	2.02	1.79	1.01	1.47	1.64	1.56	1.43
Framelet	1.14	1.67	1.71	1.62	1.51	0.91	1.19	1.23	1.19	1.14
deconvblind	0.81	0.92	1.02	1.07	1.10	0.67	0.78	0.85	0.89	0.91
Nonlocal TV	0.74	0.85	0.92	0.69	0.59	0.62	0.62	0.61	0.57	0.53

Table 1. Comparison of ISNRs for each method using images with various noise levels and imperfect PSFs. The input PSF satisfies $\tilde{h} = h^k$ where h is the exact PSF.

In the second experiment, we tested the random circles which mimic the pits on the cell membrane. Aside from the difference of the pattern, the simulated data was generated in the same manner with that for the first experiment. We show the results by testing the blurry image with Gaussian noise $\sigma = 6$ and $k = 0.6$ for PSF $\tilde{h}$ in Fig. 3. It is clear that two adjacent circles are separated in our result with minimal artifacts along the structure. However, they are merged in the result by using the Richardson-Lucy's method. In this case, nonlocal TV suffers from the ringing artifacts along the boundaries. Similar to the first experiment, the framelet result has huge artifacts and thereby has the lowest ISNR score among all results.

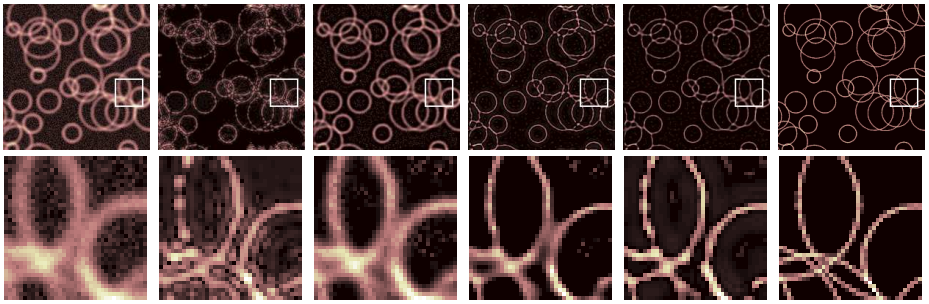

Fig. 3. Deconvolution of a blurry image with noise and imperfect PSF. From left to right: input blurry image, nonlocal TV (ISNR=0.91), "deconvblind" (ISNR=1.19), Richardson-Lucy (ISNR=2.96), the proposed result (ISNR=3.68), and the ground truth.

4 Conclusions

A novel regularization based image deconvolution model for fluorescence microscopy images has been proposed in the paper. To preserve the various directional structures of the image, the shearlet transform as a multiscale representation system with high accuracy is employed in the model. Addressing the dynamic range and various smoothness orders, TGV serves as a regularization term to reduce the noise and staircase effects. The proposed model is solved efficiently by applying ADMM, and thereby fast convergence is guaranteed. Numerical results show that our proposed approach is particularly advantageous for deblurring fluorescence microscopy images in terms of ISNR and visual quality compared to other state-of-the-art methods.

Acknowledgments

The first and second authors would like to thank the helpful discussions with Giang Tran from Department of Mathematics at UCLA. The research of Jing Qin and Stanley Osher was supported by a grant from the Keck foundation.

This work of Xiyu Yi and Shimon Weiss was supported by NIH grant No. 5R01EB000312.

References

1. T. Dertinger, R. Colyer, G. Iyer, S. Weiss, and J. Enderlein. Fast, background-free, 3D super-resolution optical fluctuation imaging (SOFI). *Proceedings of the National Academy of Sciences*, 106(52):22287–22292, 2009.
2. R. C. Gonzalez, R. E. Woods, and S. L. Eddins. *Digital image processing using MATLAB*. Pearson Education India, 2004.
3. W. H. Richardson. Bayesian-based iterative method of image restoration. *JOSA*, 62(1):55–59, 1972.
4. L. B. Lucy. An iterative technique for the rectification of observed distributions. *The astronomical journal*, 79:745, 1974.
5. T. F. Chan and C. K. Wong. Total variation blind deconvolution. *Image Processing, IEEE Transactions on*, 7(3):370–375, 1998.
6. X. Zhang, M. Burger, X. Bresson, and S. Osher. Bregmanized nonlocal regularization for deconvolution and sparse reconstruction. *SIAM Journal on Imaging Sciences*, 3(3):253–276, 2010.
7. J. L. Starck, M. K. Nguyen, and F. Murtagh. Wavelets and curvelets for image deconvolution: a combined approach. *Signal Processing*, 83(10):2279–2283, 2003.
8. J. A. Dobrosotskaya and A. L. Bertozzi. A wavelet-laplace variational technique for image deconvolution and inpainting. *IEEE Transactions on Image Processing*, 17(5):657–663, 2008.
9. V. M. Patel, G. R. Easley, and D. M. Healy Jr. Shearlet-based deconvolution. *Image Processing, IEEE Transactions on*, 18(12):2673–2685, 2009.
10. J. F. Cai and Z. Shen. Framelet based deconvolution. *J. Comput. Math*, 28(3):289–308, 2010.
11. J. Qin and W. Guo. An Efficient Compressive Sensing MR Image Reconstruction Scheme. In *Biomedical Imaging: From Nano to Macro, IEEE International Symposium on*, pages 306–309, 2013.
12. W. Guo, J. Qin, and W. Yin. A new Detail-Preserving Regularity Scheme. *UCLA CAM Report*, 13-04, Jan. 2013.
13. T. Goldstein and S. Osher. The split bregman method for l1-regularized problems. *SIAM Journal on Imaging Sciences*, 2(2):323–343, 2009.
14. G. Kutyniok, K. Guo, and D. Labate. Sparse multidimensional representations using anisotropic dilation and shear operators. In *Wavelets und Splines (Athens, GA, 2005), G. Chen und MJ Lai, eds., Nashboro Press, Nashville, TN*, pages 189–201, 2006.
15. K. Bredies, K. Kunisch, and T. Pock. Total Generalized Variation. *SIAM Journal on Imaging Sciences*, 3(3):492–526, 2010.
16. M. S. Almeida and L. B. Almeida. Blind and semi-blind deblurring of natural images. *Image Processing, IEEE Transactions on*, 19(1):36–52, 2010.
17. T. J. Holmes, S. Bhattacharyya, J. A. Cooper, D. Hanzel, V. Krishnamurthi, W. Lin, B. Roysam, D. H. Szarowski, and J. N. Turner. Light microscopic images reconstructed by maximum likelihood deconvolution. In *Handbook of biological confocal microscopy*, pages 389–402. Springer, 1995.
18. M. S. Almeida and M. A. Figueiredo. Deconvolving images with unknown boundaries using the alternating direction method of multipliers. 2013.